Journal of Nuclear Materials 601 (2024) 155332

Contents lists available at ScienceDirect

Journal of Nuclear Materials

journal homepage: www.elsevier.com/locate/jnucmat

W-EUROFER97 brazed joints using Ag, Au, and Cu-based fillers for energy applications: A microstructural and mechanical study.

V. Díaz-Mena [a,*], J. de Prado [a], I. Izaguirre [a], J. Carreras [b], M. Sánchez [a,c], M. Rieth [d], A. Ureña [a,c]

[a] Materials Science and Engineering Area, ESCET, Universidad Rey Juan Carlos, C/Tulipán s/n, 28933 Móstoles, Madrid, Spain
[b] Materials of Energetic Interest Division, Technology Department, CIEMAT, Avenida Complutense, 40, Madrid, Spain
[c] Instituto de Tecnologías para la Sostenibilidad, Universidad Rey Juan Carlos, Spain
[d] Karlsruhe Institute of Technology, Institute for Applied Materials, Karlsruhe, Germany

GRAPHICAL ABSTRACT

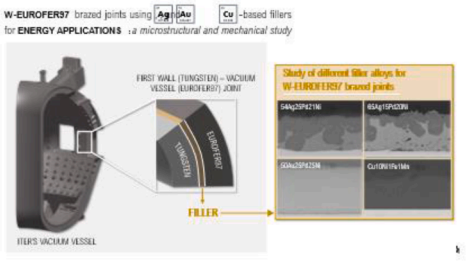

ARTICLE INFO

Keywords:
Brazing
Fusion reactor
EUROFER97
Tungsten
Characterization

ABSTRACT

The brazeability of four different alloys (Au, Cu, and two Ag-based alloys) was evaluated for their use as filler materials in joints between EUROFER 97 and tungsten for its application in future fusion reactors. The study aims to analyze the operational brazeability in terms of deep microstructural analysis and mechanical behavior.

In general, high metallic continuity was observed for all filler compositions. In the case of the joints brazed with the Au-based filler alloy, a homogeneous microstructure based on an Au-Pd-Fe-Ni solid solution is obtained. The use of Ag-based filler alloys produced a solid solution phase at the EUROFER97-braze interface, and a Ag-based phase in contact with the tungsten base material. Finally, with the cupronickel filler alloy, a braze constituted by two different Cu-Ni-Fe solid solution phases is obtained.

Regarding the mechanical characterization, the Cu-based filler shows a lower hardness value, while the higher values were obtained with one of the Ag-based filler alloy. In the case of the shear tests, a maximum 304 ± 57 MPa strength is obtained for Au-based filler alloy brazed at 1171 °C due to the combination of a homogeneous and toughness microstructure and the lack of intermetallic compounds in the braze.

* Corresponding author.
E-mail address: victor.diaz@urjc.es (V. Díaz-Mena).

https://doi.org/10.1016/j.jnucmat.2024.155332
Received 28 May 2024; Received in revised form 4 July 2024; Accepted 5 August 2024
Available online 6 August 2024

1. Introduction

Nuclear energy provides low-carbon or decarbonized electricity and can be categorized as an environmentally friendly source of clean energy since there is little or no greenhouse gas (GHG) emissions. The wide use of fission nuclear reactors has shown that the most common problems are centered on safety issues, the disposal of radioactive waste, and the limited supply of raw materials such as uranium. These concerns are not relevant to fusion reactors, as only a few grams of fuel in the reactor vessel are necessary for reactor operation, and, therefore, an uncontrolled reaction is not possible. The materials close to the fusion reactions will become radioactive but, with a careful materials selection, these materials will have a short half-life period; therefore, the waste disposal problems will be minimal [1].

The design and characterization of candidate materials for the first walls, that can survive for years in the harsh conditions of the fusion reactors [2] (which combines energetic neutrons irradiation, very high thermal loads, and intense interactions with deuterium and tritium), is crucial. The materials that will be exposed to the harshest environments in fusion power plants are those contained within the vacuum vessel. They can be broadly classified into three types: Plasma Facing Materials (PFMs; formed by the first wall and the divertor [3–7]), blanket (formed by the tritium breeder, neutron multiplier, and a shield with the coolant inside for the energy transfer [8–11]) and diagnostic materials.

The recent designs of the divertor structure consist of monoblocks of tungsten and its alloy and CuCrZr coolant pipes modules [12–14]. For the first wall structure, the component that will face the plasma consists of a tungsten layer joined to a structural Reduced Activation Ferritic Martensitic Steels (RAFMS). Currently, different RAFMs such as EUROFER97 or the F82H, and Oxide Dispersed Steels (ODS) are being developed for future application based on radiation studies carried out [15,16].

The structure of a fusion reactor is multi-component, and each component is formed by different materials, thus the development of joining technologies between dissimilar materials is necessary. More specifically, joints between tungsten (W-W) and between tungsten and EUROFER97 (W-E) are important for the above-mentioned components. Different joining techniques have been studied for several years [17,18], concluding that high-temperature brazing is one of the most promising and widely used techniques of all. This technique has the advantages of lower joining temperature, than those applied in liquid-state joining techniques, and shorter times than solid-state ones.

Many authors have studied different brazing methods and compositions of brazing alloy fillers. Among the various filler materials available, Ag, Au, Ni, and Cu-based materials have gained widespread popularity due to their excellent mechanical and chemical properties [19–25] for high-temperature applications. It is important to mention that all these elements develop a high specific activity (above 1.00×10^{14} Bq/kg) and gamma dose rate (above 1.00×10^{4} Sv/h) with a short decay time under its exposure to a neutron irradiation spectrum similar to the expected in the fusion. However, the combination of the great brazeability that shows those filler alloys and the fact their applications only suppose a few microns layer in the component, their use as filler alloys is gaining interest in the scientific community. W-EUROFER97 joints using those filler alloys are characterized by interesting properties such as: (i) great wettability of the filler in the base material ensuring defect-free interfaces, (ii) producing joints with high strength and durability, (iii) helping to minimize the risk of corrosion and reduce thermal expansion mismatch and (iv) what is more important produce joints with high ductility and toughness, which offers the possibility to control or relieve thermal stresses induced by the mismatch of thermal expansion coefficients.

This study aims to investigate the performance of Ag, Au, and Cu-based fillers in brazed joints between steel and tungsten. Specifically, the study will focus on the effects of filler material type and joining conditions on the resultant microstructure and its correlation with the mechanical properties of the brazed joints. The results of this study will provide valuable insights into the design and optimization of brazed joints in various industrial applications. In addition, the complete microstructural and mechanical analysis carried out will provide information about the effect of microstructural and compositional effect of the filler/braze alloy on the mechanical properties of the joint.

2. Experimental details

2.1. Materials employed for the brazed joints

The base material used for the brazed joints were: i) $a > 99.97$ % polycrystalline tungsten commercialized by Plansee [Anon., 26]; and ii) a reduced activation ferritic/martensitic steel (EUROFER 97–2) with a chemical composition in weight percentage of 0.11C, 8.90Cr, 0.42Mn, 0.19 V, 1.10 W, 0.14Ta balanced Fe [27].

The intermediate materials used as filler were two commercial Ag alloys (Pallabraze950™, Pallabraze880™ [Anon., 28]), one Au-based (Gold Braze 5025 ™, supplied by *LOT-TEK* [Anon., 29]) and Cu-based alloy supplied by *Auerhammer Metallwerk* (Cupronickel [Anon., 30]), all of them supplied in foils form. Their chemical compositions and dimensions specified by the manufacturer are shown in Table 1.

2.2. Brazing process

Base materials were prepared by cutting them to the dimension of 5 × 5 × 5 mm^3 and grinding the exposed surfaces to P4000 grit size using silicon carbide paper to control the surface roughness. The polished surfaces were cleaned with isopropanol so minimal contamination was presented in the exposed surface before the brazing process.

A high vacuum furnace (*Nabertherm P330*) was used for the brazing tests at a residual pressure of 10^{-6} mbar. Fig. 1 shows an schematic of this process, where the arrangement of the cubes and filler material in the furnace is shown.

The effect of the brazing temperature on the microstructure and joint properties was examined by applying brazing temperatures of +25 and +50 ºC above the theoretical liquidus one for each filler alloy. In some samples, the application of the +25 ºC overheating demonstrated the consecution of high spreading capabilities, in those cases the application of brazing temperatures of +10 ºC above the theoretical one was studied to optimize the process. The heating ramp and dwell time were chosen according to previous thermal studies carried out [31,32]. Table 2 summarizes all brazing conditions applied to the different joints.

2.3. Characterization techniques

Solidus and liquidus experimental temperatures of the filler alloy were determined only in the case that the application of the above brazing temperatures did not produce the melting of the filler alloy. Then, a Differential Thermal Analysis (DTA) test in an argon atmosphere with equipment from *Setaram* (Thermic Analyzer Setsys 16/18) was conducted to determine the experimental solidus and liquidus values. The experiment consisted of a 10 °C/min heating ramp from room temperature to temperature 100 °C above the theoretical liquidus temperature. Then the sample was cooled down using the same ramp. The heat exchanges during the heating and cooling processes were recorded.

Table 1
Chemical compositions of different alloys used for the joints.

Filler alloy	Manufacturer composition (atomic percentage)	Dimensions w x t (mm^2)
Pallabraze950™	54Ag25Pd21Cu	0.1 × 109
Pallabraze880™	65Ag15Pd20Cu	0.06×16
Goldbraze5025™	50Au25Pd25Ni	0.05×12.7
Cupronickel	Cu10Ni1Fe1Mn	0.06×16

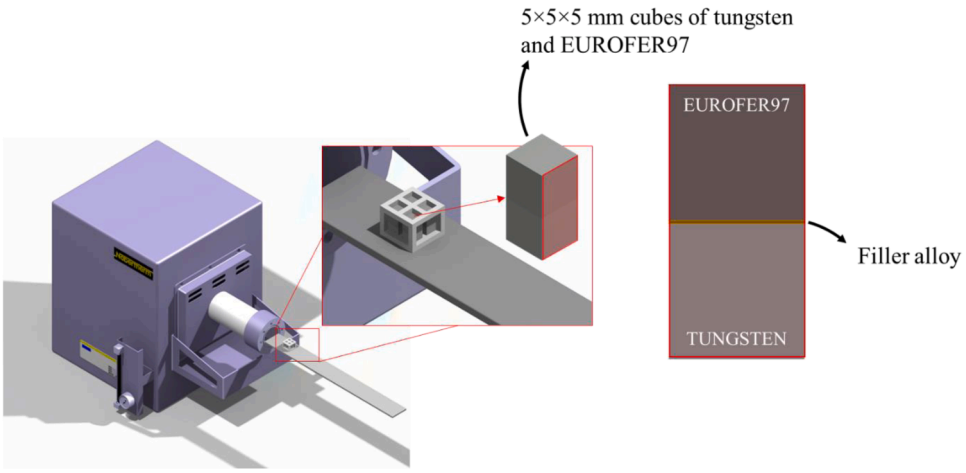

Fig. 1. 3D scheme of the brazing process inside the furnace for all the conditions manufactured.

Table 2
Temperature data and brazing conditions of each composition used.

Filler	Solidus temperature (°C)	Liquidus temperature (°C)	Brazing temperature (°C)	Dwell time (min)
54Ag25Pd21Cu	901	950	950 + 50	10
			950 + 25	10
			950 + 10	10
			950 + 10	5
65Ag15Pd20Cu	856	880	880 + 50	10
			880 + 25	10
50Au25Pd25Ni	1101	1121	1121 + 50	10
			1121 + 25	10
Cu10Ni1Fe1Mn	1170	1193	1193 + 50	10
			1193 + 25	10
			1193 + 10	10

The experimental composition of the filler material was determined by X-ray fluorescence spectroscopy (XRF, *Philips Magix Pro*) for comparison purposes with the composition provided by the manufacturer in the specification sheet.

Metallographic examination of the brazed joints was made in the cross-section cut, following a standard polishing technique preparation procedure. The main microstructural analysis was carried out using Scanning Electron Microscopy (SEM, *S3400 Hitachi*) equipped with EDX. The main target of this characterization is to obtain information about the metallurgical continuity (operational weldability) and phase distribution obtained with the thermal conditions imposed. The metallurgical interaction between the filler alloy and base materials (especially EUROFER97), that occurs during the brazing process, was also studied.

The mechanical properties of the joints were evaluated with microhardness and shear tests. The hardness study was carried out by tracing a profile across the joints with *MHV-2SHIMADZU* equipment. This study gives information about the effect of the brazing process on the hardness properties of the base materials. A 100 g ($HV_{0.1}$) load was applied for 30 s following the *ASTM: E384–11 Standard Test Method for Knoop and Vickers Hardness of Materials* [Anon., 33]. Distances between neighbor indentations were longer than three times the residual imprint sizes.

Shear strength values were obtained using a shear fixture that was placed between compress plates in a Universal Testing Machine (*Zwick Z100*) at a speed of 1 mm/min. In this case, only samples where high wettability and metallurgical continuity were achieved, were considered for these tests. The characterization of the shear fracture surface was carried out by SEM and stereoscopic microscope *Leica DMR* equipped with Leica Image Pro Plus software. Both mechanical tests, hardness, and shear, were performed at 25 ºC.

3. Results

3.1. Compositional characterization of the filler alloys

The composition of filler alloys, determined by X-Ray Fluorescence Spectroscopy (XRF) is shown in Table 3. It shows the compositions in weight percentage compared with the theoretical ones provided by the manufacturer. Some variations between both compositions were found. For example, in the 54Ag25Pd21Cu filler alloy, the Ag content measured by XRF was almost 5 % higher than the specified by the manufacturer. The weight percentage of Cu was also higher, while the Pd was much lower than the specified value. Ag content in the 65Ag15Pd20Cu filler was also higher than the specification, but for Pd and Cu the wt.% measured was lower. Regarding the composition of the 50Au25Pd25Ni filler, both the Pd and Ni contents were higher when measured by XRF, but not in the case of Au. In the case of the Cu10Ni1Fe1Mn filler, the experimental composition agrees with that specified by the manufacturer.

3.2. Microstructural characterization of brazed joints

3.2.1. W-EUROFER97 joints with 50Au25Pd25Ni filler alloy

Fig. 2 shows the microstructure of the brazed joints made with this filler alloy for both tested brazing temperatures over the theoretical liquidus one 1121 + 25 ºC (1146 ºC) and 1121 + 50 ºC (1171 ºC). A microstructure consisting of a solid solution of the elements that constitute the filler alloy is obtained. Then, a homogeneous braze formation of approximately 70 and 44 μm. width for 1146 and 1171 ºC brazing temperature, respectively is obtained.

However, some interactions between the braze and both base materials have been detected at both interfaces. To analyze the nature of the different phase formations at the interfaces, a semiquantitative composition determination by EDX punctual analysis was performed and shown in Fig. 3 for the 1146 ºC condition. The analysis of both the general microstructure and the two interfaces will be conducted on the Discussion section.

3.2.2. W-EUROFER97 joints with Cu10Ni1Fe1Mn filler alloy

The characterization of the W-EUROFER97 joints brazed with Cu-Ni filler alloy shows that the application on + 25 ºC overheating above the theoretical liquidus temperature did not produce the melting of the braze. To determine the experimental liquidus temperature a DTA (Differential Thermal Analysis) was carried out to serve as a reference liquidus temperature for the brazing conditions. The experimental solidus and liquidus temperatures extracted from de DTA cooling curve were 1170 and 1193 ºC, respectively, as shown in Fig. 4.

Table 3
Comparison between composition given on the datasheet and XRF measurements.

		Composition in weight percentage.						
		Ag	**Pd**	**Cu**	**Ni**	**Au**	**Fe**	**Mn**
54Ag25Pd21Cu	**Specification sheet**	54.00	25.00	21.00	–	–	–	–
	XRF	59.60	16.40	24.00	–	–	–	–
65Ag15Pd20Cu	**Specification sheet**	65.00	15.00	20.00	–	–	–	–
	XRF	68.30	13.40	18.30	–	–	–	–
50Au25Pd25Ni	**Specification sheet**	–	25.00	–	20.00	50.00	–	–
	XRF	–	27.60	–	26.20	46.20		
Cu10Ni1Fe1Mn	**Specification sheet**	–	–	88.00	10.00	–	1.00	1.00
	XRF	–	–	87.40	10.30	–	1.61	0.68

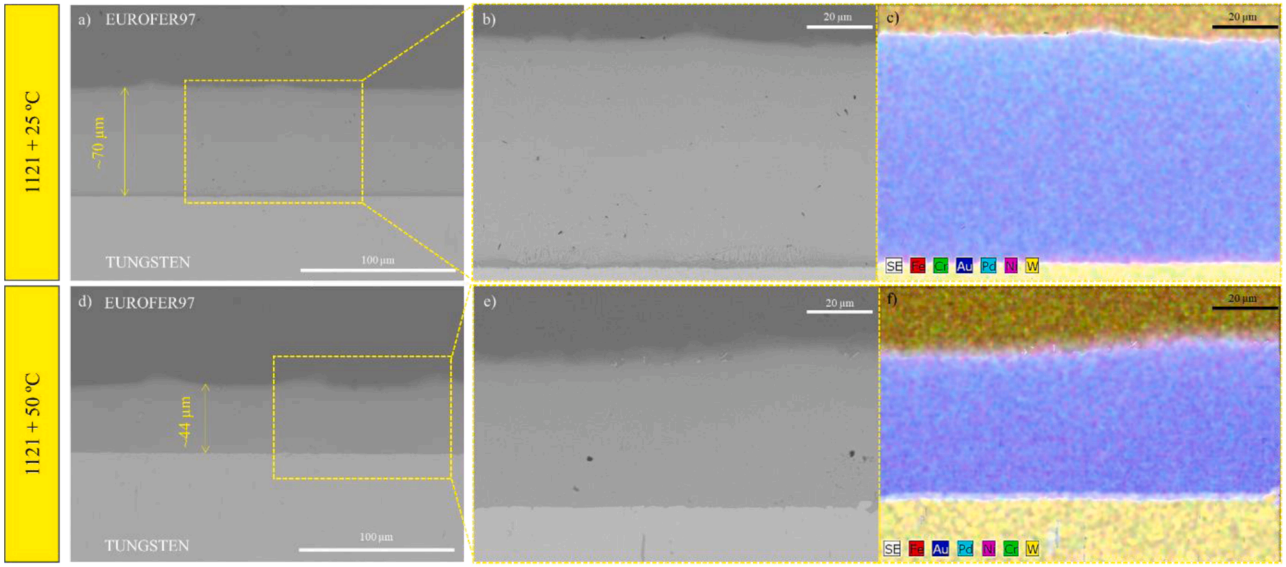

Fig. 2. SEM-BSE images for the EUROFER97-W joints brazed with 50Au25Pd25Ni filler at a)- c) 1146 °C and d) - f) 1171 °C.

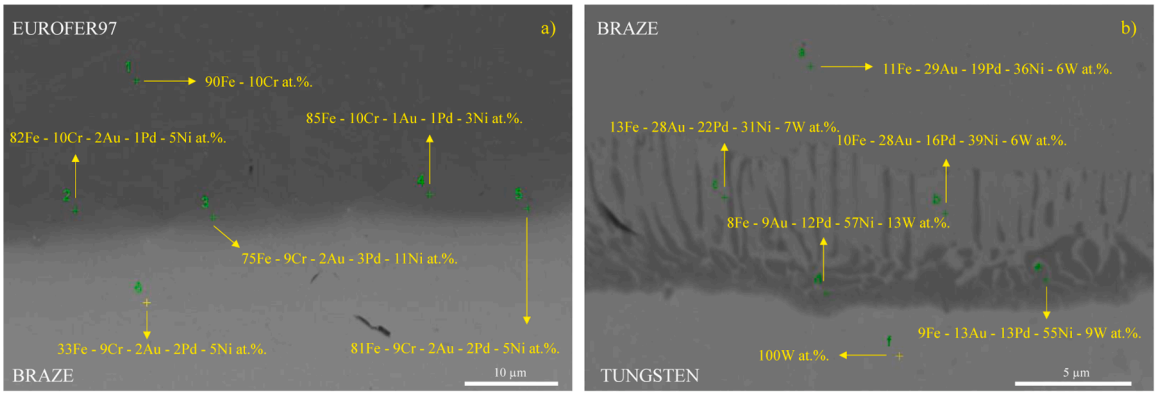

Fig. 3. Detail micrographs of both interfaces indicating the position of the EDS analyses in each case a) EUROFER97 interface and b) tungsten interface of the brazed joint with 50Au25Pd25Ni at 1146 °C.

Fig. 5 shows the different microstructures obtained with this alloy, after applying the new experimental liquidus temperature for the brazing tests. In this case, the excellent wettability showed by the filler under both overheating conditions 1193 + 25 °C (1218 °C) and 1193 + 50 °C (1243 °C) produce the exudation of the braze out of the joint clearance. Therefore, 1193 + 10 °C (1203 °C) condition was also studied in trying to optimize the brazing process.

Although in principle, the backscattering images of Fig. 5 show the consecution of a homogenous braze composition, after etching, the presence of different phases inside the braze was revealed. As in the case of the joints with the previously described filler metal, the interfaces between the base materials and the brazing alloy are of particular interest, as there appears to be a nickel enrichment at both interfaces. A detailed analysis of these Ni-rich diffusion phases formed at both interfaces for the + 50 °C condition is shown in Fig. 6.

3.2.3. W-EUROFER97 joints with 54Ag25Pd21Cu filler alloy

W-EUROFER97 using Ag-Cu-Pd filler alloys have been widely applied as brazing alloys, but their microstructure has been rarely reported. Fig. 7 shows general micrographs of the brazed zone carried out

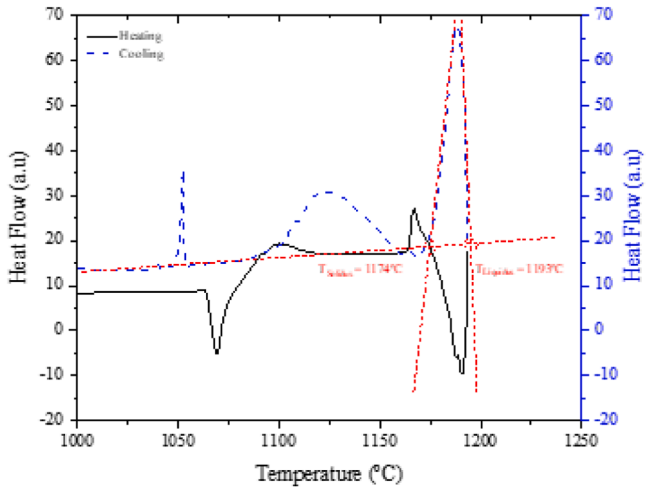

Fig. 4. Thermogram obtained from the DTA analysis carried out in the Cu10Ni1Fe1Mn filler alloy.

with the 54Ag25Pd21Cu alloy for both conditions (975 ºC and 1000 ºC, respectively). The main difference between conditions is the appearance of porosity at the braze-tungsten interface in the 1000 ºC condition.

Due to the higher metallurgical continuity achieved using the lower brazing temperature and the exudation of the filler occurred during the brazing process, an overheating of + 10 ºC (960 ºC) over the liquidus temperature varying the dwell time (5 and 10 min) was carried out to determine its effect in the brazeability of the joint. Fig. 8 shows the resultant microstructures for both conditions, where it can be observed that a similar microstructure was obtained.

3.2.4. W-EUROFER97 joints with 65Ag15Pd20Cu filler alloy

Joints brazed at (+ 25 and + 50 ºC; 905 and 930 °C, respectively) with this filler alloy are shown in Fig. 9. The results indicated the consecution of metallurgical continuity in both cases. The higher Ag content of this filler results in a higher proportion of the Ag-rich phase in the braze.

3.3. Mechanical characterization of the joints

3.3.1. Hardness characterization

Fig. 10a)–d) show the hardness profiles across the brazed joint thickness for the different brazed joints. The braze with the highest hardness value is the 54Ag25Pd21Cu, with the 975 and 1000 ºC conditions having values of 408.33 ± 3.05 and 360.66 ± 17.21 $HV_{0.1}$, respectively.

Two joints brazed with 54Ag25Pd21Cu and 50Au25Pd25Ni fillers were etched to reveal the microstructure in order to analyse the effects of brazing below and above the EUROFER97 austenitisation field on the mechanical properties. Fig. 11 shows these microstructures, where the presence of two different microstructures based on ferrite + martensite (1121 + 25 ºC) and ferrite + pearlite (880 + 25 ºC) are observed.

3.3.2. Shear strength tests

For this characterization, only conditions that showed the best brazeability for each filler alloy in the microstructural characterization were selected for these tests. Those conditions are listed in Table 4.

Fig. 12 shows the results of the shear tests and Fig. 13 shows the different fracture surfaces for each filler and condition. W-EUROFER97 joints brazed using 50Au25Pd25Ni filler alloy show the highest shear strength among all conditions (304 ± 57 MPa). By using Cu10Ni1Fe1Mn filler alloy for brazing W to EUROFER97 produce joints with a shear strength of 196 ± 34 MPa. Finally, the use of the Pallabraze alloys (54Ag25Pd21Cu and 65Ag15Pd20Cu), showed the lowest strength results (119 ± 4 MPa and 118 ± 1 for 54Ag25Pd21Cu and 65Ag15Pd20Cu, respectively).

4. Discussion

Here, the results presented in the above-mentioned section will be discussed. The section is divided into the discussion of the microstructural characterization first and, then, the mechanical characterization of the joints.

4.1. Microstructural characterization of the joints

4.1.1. 50Au25Pd25Ni joints

The reduction of the braze thickness observed between the two conditions studied and shown in Fig. 2 is associated with the increase of the wettability, fluidity, and exudation of the braze alloy with the temperature. This generates a loss of filler at the edges of the base materials due to capillary action.

The study of the EUROFER97 – braze interface (Fig. 3a)) shows the formation of a diffusion layer associated with the diffusion of Ni from the braze to the joint interface. In addition, the presence of Fe and Cr in the proximity of the braze with the interface indicated that those elements had been dissolved from the EUROFER 97 and penetrated the braze during the heating stage.

The tungsten-braze interface is less smooth, and it is characterized by the formation of an interaction layer of approximately 6 μm thick, where the presence of a eutectic-like microstructure is observed (Fig. 3b)). This layer is constituted by two phases with Fe-Au-Pd-Ni-W composition, where the darker phase is richer in Ni content, as was previously reported by Y. K. Yu et al. [34] in brazed joints between Inconel 601 and 422 stainless steels with a 70Au – 22Ni – 8Pd alloy filler. The Fe dissolved from the EUROFER97 diffuses along the whole braze to interact with W at the bottom interface giving rise to the studied phases.

4.1.2. Cu10Ni1Fe1Mn joints

For this filler alloy, three brazing temperatures were conducted and showed in Fig. 5. All the joints were continuous, showing only some black dots that could be associated with micrometric porosity, which could be attributed to the solidification process of the molten filler. The wave-like top interface with EUROFER97 demonstrates that the filler tends to penetrate through the grain boundary of the EUROFER97 (with arrow in Fig. 5a) and b)). This phenomenon has been previously reported by other authors when they braze W to EUROFER97 using Cu fillers at temperatures slightly lower than those used in the present study [23,35].

Fig. 6 shows the two interfaces with base material for the + 50 ºC condition, appreciated after chemical etching. In the case of the EUROFER97-braze interface, the interdiffusion of elements from EUROFER97 and the braze gave rise to the formation of a diffusion layer approximately 10 μm thick. These layers have an average composition rich in iron with some incorporation of Cu and Ni, as the EDS punctual analysis indicated. However, the solid-state diffusion nature produces differences in composition as it approximates the EUROFER97 or the braze. In the case of the W-braze interface the formation of phase with approximate composition in atomic percentage 25Cu-25Ni-50Fe is detected. This phase tends to solidify in contact with tungsten base material forming a layer and, at some points, it penetrates or solidifies inside the braze, as the element mapping composition and Fig. 6 show.

4.1.3. 54Ag25Pd21Cu joints

Both joints conducted with this filler alloy show the formation of similar phases inside the braze formed by the segregation of Ag from the Cu and Pd, forming two different phases: i) an Ag-rich phase in direct contact with the bottom base material (tungsten) and as isolated spheres distributed along the braze width, and ii) a Pd-Cu solid solution phase above the Ag-rich one in contact with the top base material

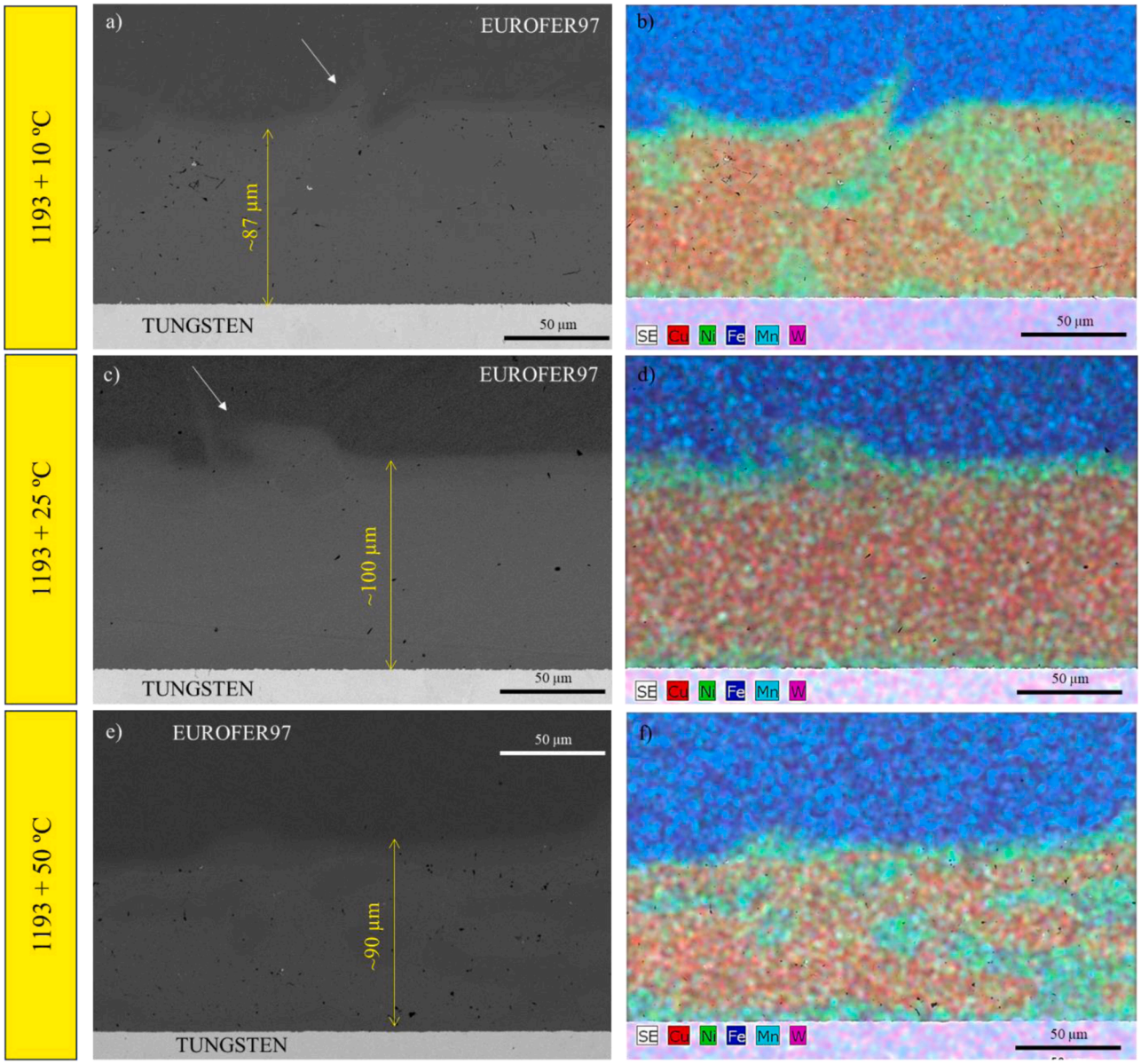

Fig. 5. SEM-BSE images of the W-EUROFER97 joints brazed with Cu10Ni1Fe1Mn filler at a) - b) 1203 °C, c) - d) 1218 °C, and e) - f) at 1243 ºC.

(EUROFER97).

The formation of this segregation phenomenon has been previously reported and discussed by R. K. Choudhary et al. [36] in stainless steel – copper brazed joints with an Ag-Cu-Pd filler alloy (Palcusil-5). The phase segregation can be attributed to the solubility of each element present in the alloy in the melt state. Cu and Pd are completely soluble in the liquid phase and form a continuous solid solution, the same phenomenon occurs between Ag and Pd. Therefore, the solidification occurred in different melting ranges producing the observed microstructure.

In the case of the Pd-Cu rich phase, during the brazing process, the elements diffuse into the EUROFER97 base material forming a diffusion layer at this interface, due to the higher solubility of Cu in Fe than Ag in Fe. On the other hand, the interface with tungsten is well-defined, and almost no metallurgical interaction between the base material and the braze is observed at the studied temperatures.

The microstructure observed with the + 10 ºC joints conducted still consisting of an Ag-rich phase in direct contact with tungsten base material and a Pd-Cu solid solution phase above the Ag-rich one, in contact with EUROFER97 base material. The main difference between the 960 ºC and the other conditions is the less atomic percentage of Fe found in the Pd-Cu phase, since less brazing temperature may promote a less severe diffusion of the elements from EUROFER97.

4.1.4. *65Ag15Pd20Cu joints*

As in the previous case with the 54Ag25Pd21Cu, here again, a formation and segregation of an Ag-rich phase is observed at the interface with tungsten, but a Cu enrichment occurs around the Ag-rich phase. In addition, during the cooling stage, the lower quantity of Pd in the braze alloy produces an excess of Cu in the Cu-Pd solid solution which tends to segregate during the solidification in the surrounding areas of the Ag-rich phase. This phenomenon tends to increase as the brazing temperature also does, as Fig. 9c) and f) show.

4.2. *Mechanical characterization of the joints*

4.2.1. *Hardness characterization*

Observing the different hardness profiles shown in Fig. 10a)–d), several conclusions can be extracted.

Regarding the harness value of the tungsten base material, all joints show a similar tungsten hardness value of 449 ± 17 HV. This result

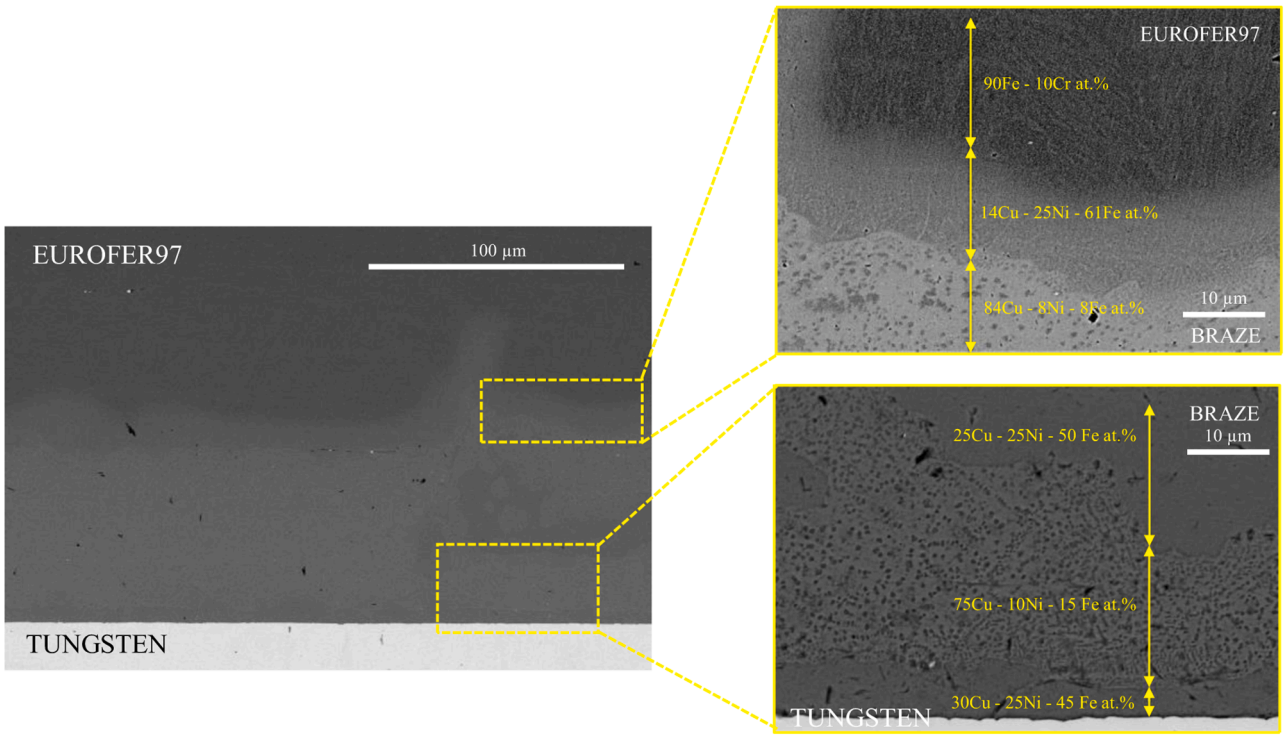

Fig. 6. Detailed images of both interfaces in W-ERUFOER97 joints brazed with Cu10Ni1Fe1Mn filler at 1243 ºC, EUROFER97-braze (upper zoomed image) and tungsten-braze (bottom zoomed image).

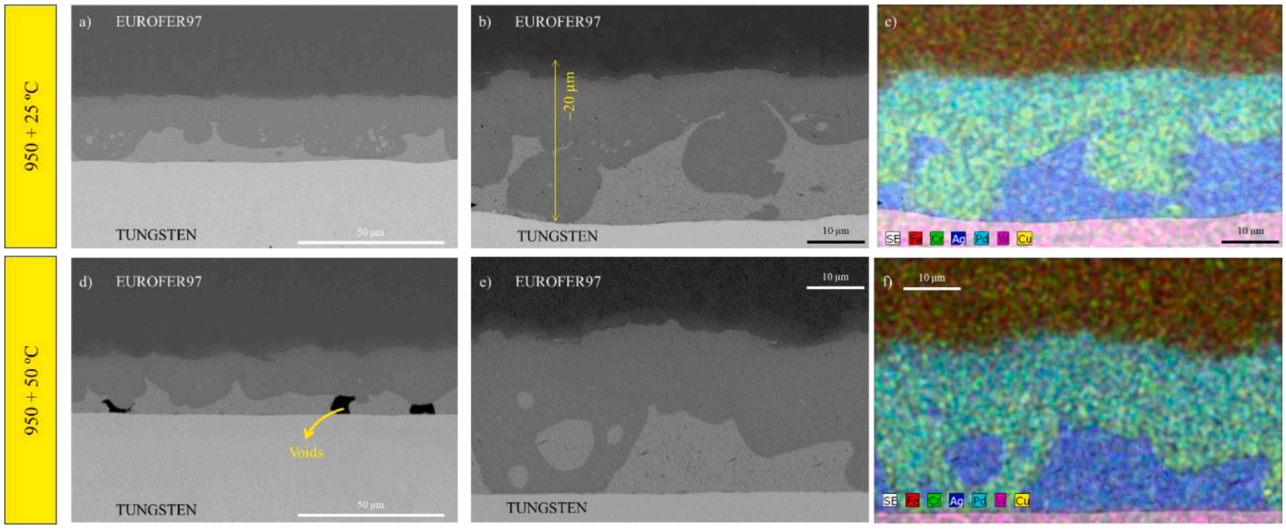

Fig. 7. SEM-BSE images and element mapping distribution of W-EUROFER 97 joints brazed with 54Ag25Pd21Cu filler at a) – b) 975 °C and c) – d) 1000 °C.

indicated that the process has not modified the hardness for any of the conditions applied, in agreement with the literature [27]. The lack of metallurgical interaction shown in the microstructural sections explains this fact.

EUROFER97 base material experimented with variations among the different conditions. In the joints brazed with the 50Au25Pd25Ni, Cu10Ni1Fe1Mn, and 54Ag25Pd21Cu (+25 and +50 ºC conditions) fillers (Fig. 10a)–c) respectively), the brazing conditions carried out situated the EUROFER97 above its austenitization field (A_{1c}=980 °C). During the cooling stage, the applied cooling rate is high enough to produce the martensite transformation and higher hardness is obtained. However, joints brazed using 905, 930, and 960 ºC with the 54Ag25Pd21Cu and the 65Ag15Pd20Cu joints (Fig. 10d)) did not reach the austenitization temperature during the brazing procedure, therefore lower hardness values are obtained, since the brazing process acts as an annealing treatment, where the EUROFER97 experimented a severe annealing process that causes the transformation of the martensitic microstructure to the equilibrium one, constituted by ferritic, perlitic, and a high density of precipitation carbides [27]. This can be observed in Fig. 11, where two conditions, one above the A_{1c} and another below it, were etched and analyzed under an optical microscope. In the condition brazed above the A_{1c} (1121 + 25 ºC), the martensite can be observed, while for the other condition (880 + 25 ºC), ferrite and pearlite grains are observed, explaining the lower hardness achieved for this condition.

Regarding the results obtained with each filler at the braze thickness, it can be noticed that the Cu10Ni1Fe1Mn filler shows a lower hardness

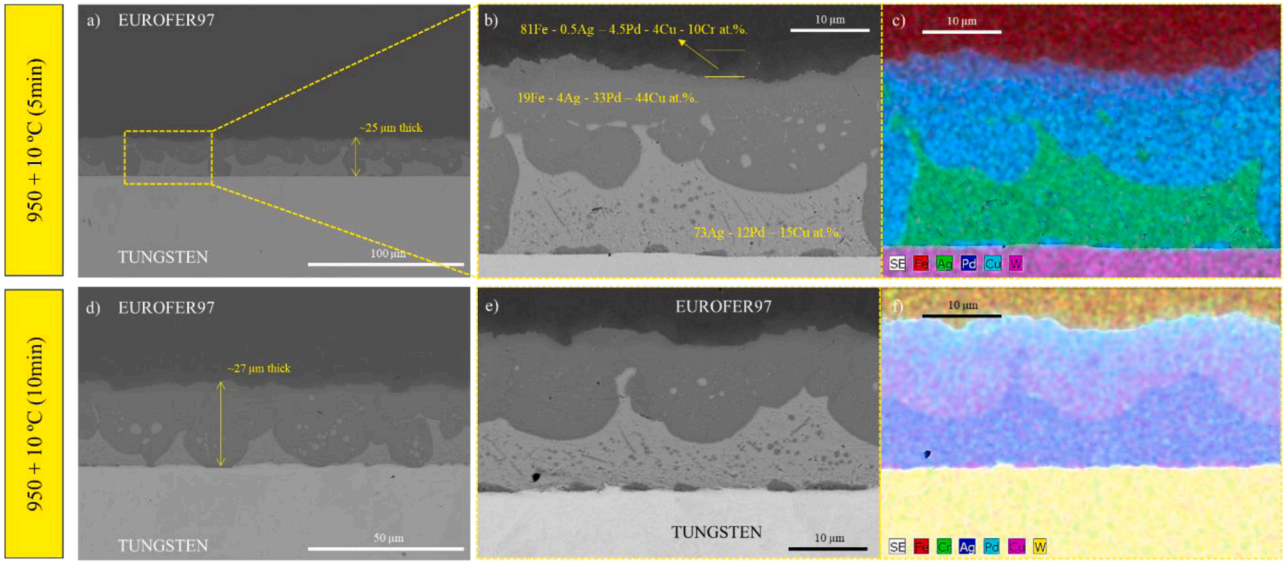

Fig. 8. SEM-BSE images of W-EUFOER 97 joints brazed with 54Ag25Pd21Cu filler at 960 °C for a) - c) 5 min, and d) - f) 10 min.

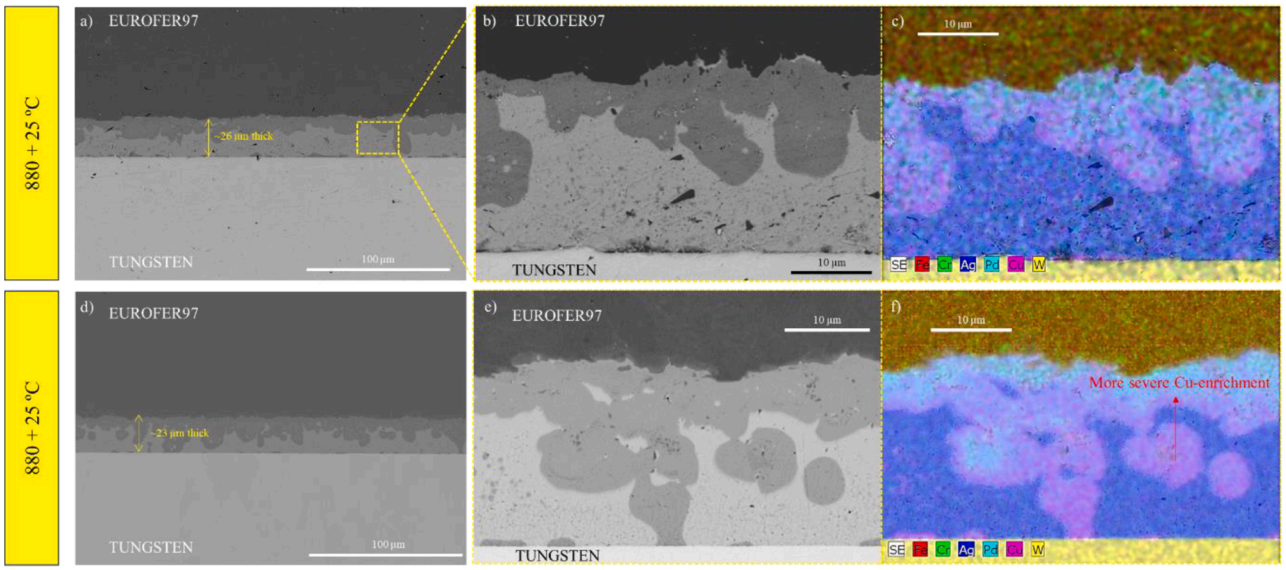

Fig. 9. SEM-BSE images for 65Ag15Pd20Cu filler at a), b), c) 905 °C and d), e), f) 930 °C.

value. This phenomenon may be directly related to the obtained microstructure, which is characterized by the formation of a solid solution with the absence of intermetallic compounds. The higher values obtained with the 54Ag25Pd21Cu could be related to the participation of Fe migrating from the EUROFER97 base material to the braze.

4.2.2. *Shear characterization*

Based on the results of shear strength observed in Fig. 12, the combination of different factors could explain the highest values obtained with the 50Au25Pd25Ni filler alloy. These factors include the formation of a homogenous braze composition by solid solution of the elements that constitute the filler alloy, the lack of intermetallic compounds in the braze, and the ductility that characterized the elements of the alloy gave rise to this high strength. The selection of the proper brazing condition means that brittle fracture is avoided because of the two last above-exposed factors, and its combination with the high metallic continuity free of brazing defects, produces a braze joint with these mechanical properties.

Analyzing the fracture surface (Fig. 13b)), the fracture started in the tungsten base material, due to the toughness character of the braze and the high adhesion properties of the braze/base material interfaces. However, at some point, the fracture propagation shifted to the braze alloy showing more participation of the filler alloy in the crack propagation of the joint, but still in its majority a substrate failure. The obtained results are like those obtained by Y. K. Yu et al. [34] using 70Au – 22Ni – 8Pd filler alloy with Inconel 601 and 422 stainless steel, where a value of 360 MPa was achieved when brazing at 1100 °C by infrared heating.

Regarding the Cu10Ni1Fe1Mn filler alloy, it also produces a homogenous braze composition, however, the formation of the Ni-rich reaction layers at both interfaces, described in the microstructural section, could explain the lower strength compared to the previous composition. The fracture surface (Fig. 13c)) showed that in this case a cohesive failure is presented, with the crack initiation and propagation through the braze and not the base material. This behavior could be associated with the high interaction achieved with the EUROFER97 and the explained reaction layer at the interfaces.

Finally, with the 54Ag25Pd21Cu and 65Ag15Pd20Cu filler alloys,

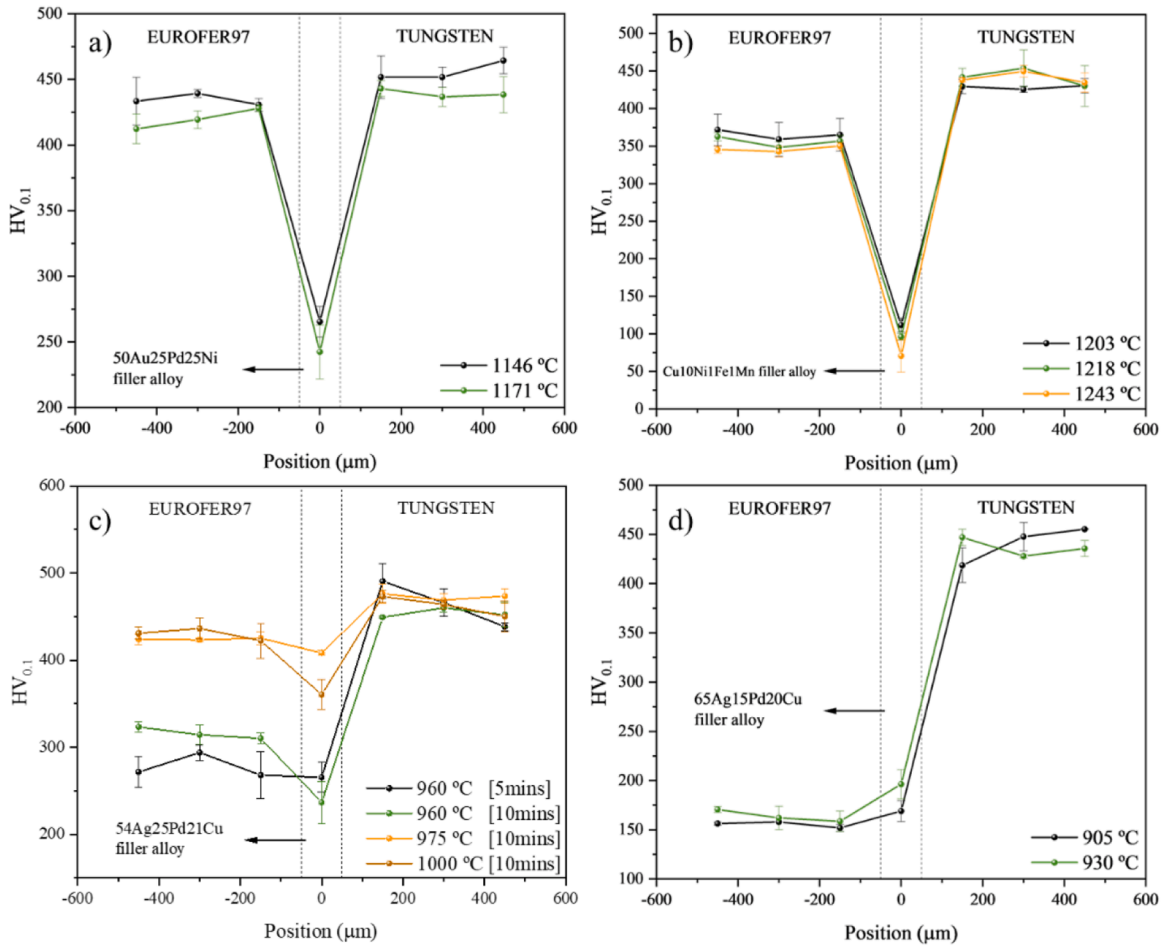

Fig. 10. Vickers hardness evolution from upper base material to bottom base material of joints brazed with a) 50Au25Pd25Ni, b) Cu10Ni1Fe1Mn, c) 54Ag25Pd21Cu, and d) 65Ag15Pd20Cu.

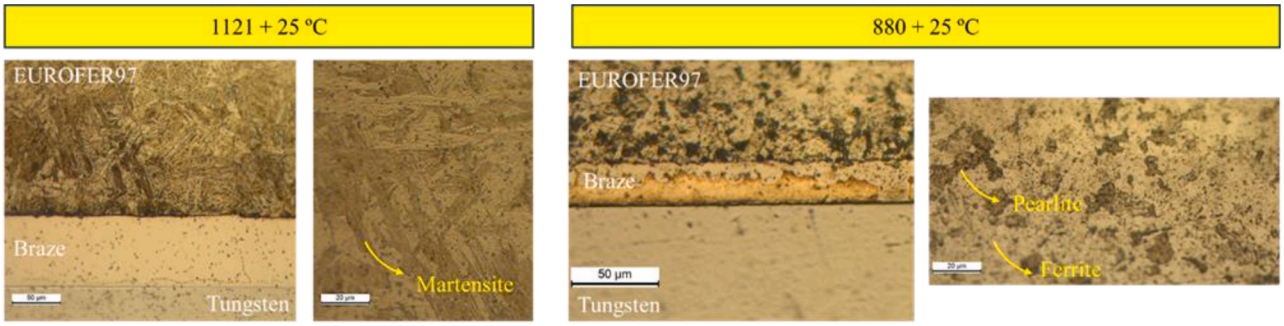

Fig. 11. Base material microstructure after brazing using two conditions: above (1121 + 25 °C) and below (880 + 25 °C) the A_{1c} temperature. Both joints were etched with 10 mL of HNO_3, 30 mL of HCl, and 30 ml of glycerol.

Table 4
Conditions selected of each filler alloy for the shear strength tests.

Filler	Condition/s tested
50Au25Pd25Ni	1121 + 50 °C (10 min)
Cu10Ni1Fe1Mn	1193 + 50 °C (10 min)
54Ag25Pd21Cu	950 + 10 °C (5 min)
65Ag15Pd20Cu	880 + 25 °C (10 min)

the formation of the biphasic braze microstructure gave rise to an overall higher hardness, which can be attributed to more brittle mechanical behavior. The analyses of the fracture surfaces also show a cohesive failure since both base material surfaces are covered with filler alloy. In the case of the 65Ag15Pd20Cu brazed joint Fig. 13e) the fracture surface experimented with a modification of the fracture mode, participating in both interfaces. Both results are in concordance with previously reported results [36].

5. Conclusions

Brazed joints between tungsten and EUROFER97 were carried out using four different brazing alloys (Au, Cu and two Ag-based alloys). The brazeability of these four brazing alloys was evaluated for their use as filler materials for its application in future fusion reactors, the

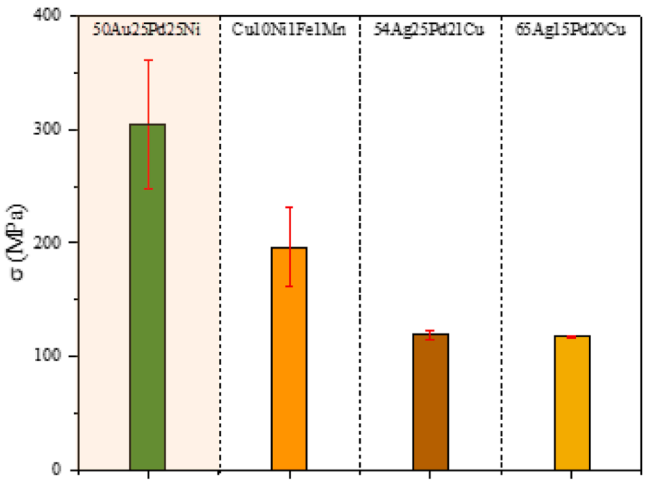

Fig. 12. Shear strength values for the different brazing fillers and conditions.

microstructural and mechanical analysis was carried out. In terms of brazeability and metallurgical continuity, all conditions studied for each filler showed high continuity. For Au-based filler alloy (50Au25Pd25Ni), the homogeneous microstructure based on an Au-Pd-Fe-Ni solid solution was obtained for the two conditions studied. Both Ag-based filler alloys (54Ag25Pd21Cu and 65Ag15Pd20Cu) produced a phase separation phenomenon during the brazing cycle, which gave a heterogeneous braze with continuity between each phase. The main difference between the brazed joints with these two fillers was the Cu-enrichment around the Ag-based phase in the 65Ag15Pd20Cu. Finally, in the case of the cupronickel filler alloy (Cu10Ni1Fe1Mn), a braze constituted by two different Cu-Ni-Fe solid solution phases was obtained.

The mechanical characterization of the joints, in terms of hardness, showed that the braze filler which gives the highest hardness was the 54Ag25Pd21Cu filler, with the 975 and 1000 ºC conditions (408.33 ± 3.05 and 360.66 ± 17.21 $HV_{0.1}$, respectively). This could be associated with the migration of Fe from the EUROFER97 base material to the braze at higher brazing temperatures. In terms of shear strength, joints brazed using 50Au25Pd25Ni filler alloy have the highest shear strength among all conditions (304 ± 57 MPa). This could be associated with the formation of a homogenous braze composition by solid solution, the lack of intermetallic compounds in the braze, and the ductility of the elements

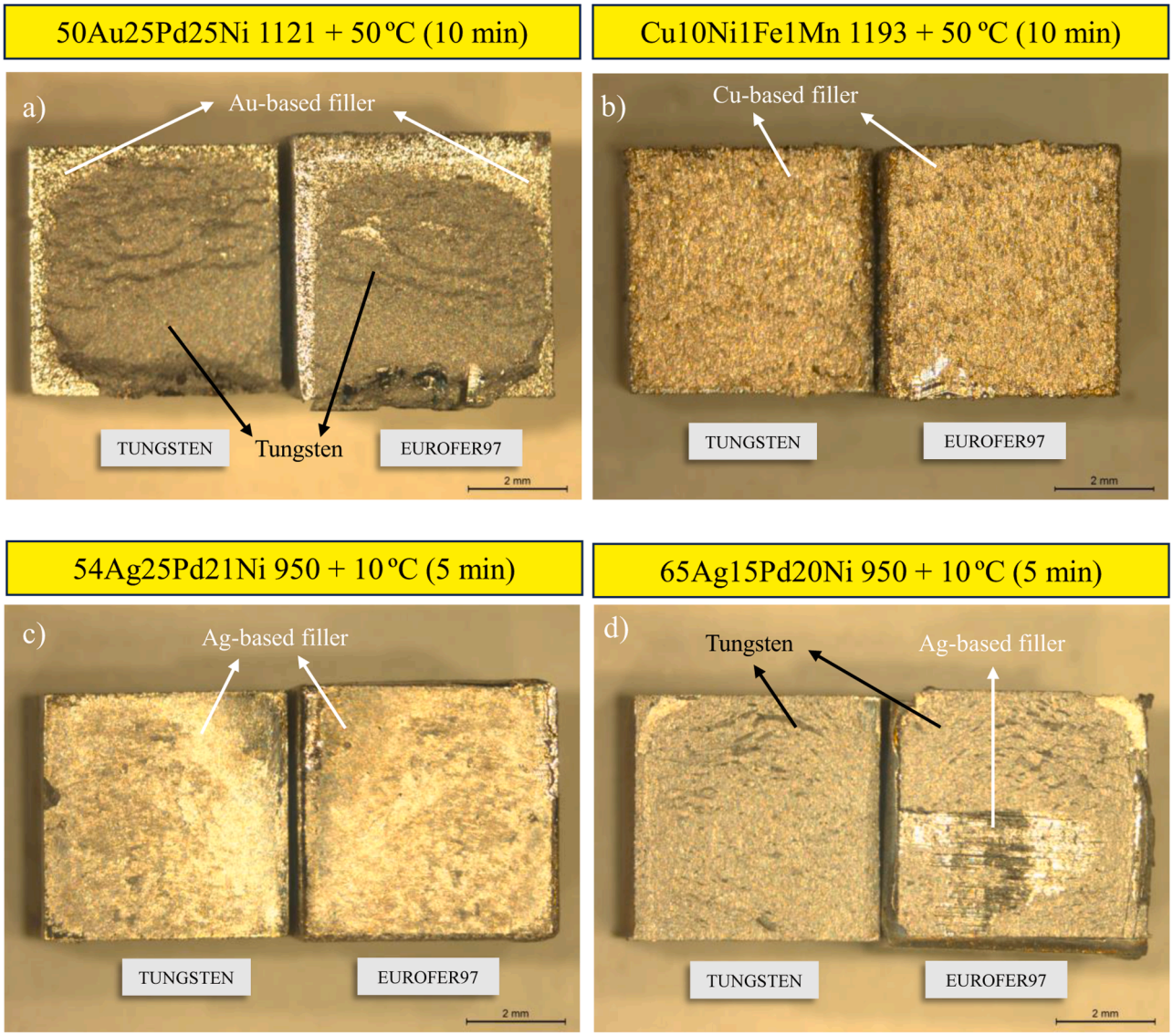

Fig. 13. Fracture surfaces for the joints carried out with the different filler alloys.

of the alloy.

CRediT authorship contribution statement

V. Díaz-Mena: Writing – original draft, Methodology, Investigation. **J. de Prado:** Writing – review & editing, Validation, Supervision, Resources, Investigation, Funding acquisition, Formal analysis. **I. Izaguirre:** Writing – review & editing, Validation, Methodology, Investigation, Formal analysis. **J. Carreras:** Methodology, Investigation. **M. Sánchez:** Writing – review & editing, Validation, Supervision, Resources, Project administration, Funding acquisition, Conceptualization. **M. Rieth:** Validation, Resources, Project administration, Funding acquisition, Conceptualization. **A. Ureña:** Validation, Supervision, Resources, Project administration, Funding acquisition, Conceptualization.

Declaration of competing interest

The authors declare that they have no known competing financial interests or personal relationships that could have appeared to influence the work reported in this paper.

Acknowledgments

This work has been carried out within the framework of the EUROfusion Consortium, funded by the European Union via the Euratom Research and Training Programme (grant agreement no. 101052200 — EUROfusion). Views and opinions expressed are however those of the author(s) only and do not necessarily reflect those of the European Union or the European Commission. Neither the European Union nor the European Commission can be held responsible for them.

References

[1] D.M. Duffy, Fusion power: a challenge for materials science, Philosophical Transactions of the Royal Society A: mathematical, Phys. Eng. Sci. 368 (2010) 3315–3328, https://doi.org/10.1098/rsta.2010.0060.
[2] B.G. Hong, W. Cho, Neutronic analysis of effects of inboard materials on the size of a tokamak fusion reactor, Nucl. Mater. Energy 28 (2021) 101040, https://doi.org/10.1016/J.NME.2021.101040.
[3] J.H. You, E. Visca, C. Bachmann, T. Barrett, F. Crescenzi, M. Fursdon, H. Greuner, D. Guilhem, P. Languille, M. Li, S. McIntosh, A.v. Müller, J. Reiser, M. Richou, M. Rieth, European DEMO divertor target: operational requirements and material-design interface, Nucl. Mater. Energy 9 (2016) 171–176, https://doi.org/10.1016/j.nme.2016.02.005.
[4] F. Militello, L. Aho-Mantila, R. Ambrosino, T. Body, H. Bufferand, G. Calabro, G. Ciraolo, D. Coster, G. di Gironimo, P. Fanelli, N. Fedorczak, A. Herrmann, P. Innocente, R. Kembleton, J. Lilburne, T. Lunt, D. Marzullo, S. Merriman, D. Moulton, A.H. Nielsen, J. Omotani, G. Ramogida, H. Reimerdes, M. Reinhart, P. Ricci, F. Riva, A. Stegmeir, F. Subba, W. Suttrop, P. Tamain, M. Teschke, A. Thrysoe, W. Treutterer, S. Varoutis, M. Wensing, A. Wilde, M. Wischmeier, L. Y. Xiang, Preliminary analysis of alternative divertors for DEMO, Nucl. Mater. Energy 26 (2021), https://doi.org/10.1016/j.nme.2021.100908.
[5] R. Kembleton, M. Siccinio, F. Maviglia, F. Militello, Benefits and challenges of advanced divertor configurations in DEMO, Fus. Eng. Des. 179 (2022), https://doi.org/10.1016/j.fusengdes.2022.113120.
[6] J.H. You, G. Mazzone, E. Visca, H. Greuner, M. Fursdon, Y. Addab, C. Bachmann, T. Barrett, U. Bonavolontà, B. Böswirth, F.M. Castrovinci, C. Carelli, D. Coccorese, R. Coppola, F. Crescenzi, G. Di Gironimo, P.A. Di Maio, G. Di Mambro, F. Domptail, D. Dongiovanni, G. Dose, D. Flammini, L. Forest, P. Frosi, F. Gallay, B.E. Ghidersa, C. Harrington, K. Hunger, V. Imbriani, M. Li, A. Lukenskas, A. Maffucci, N. Mantel, D. Marzullo, T. Minniti, A.V. Müller, S. Noce, M.T. Porfiri, A. Quartararo, M. Richou, S. Roccella, D. Terentyev, A. Tincani, E. Vallone, S. Ventre, R. Villari, F. Villone, C. Vorpahl, K. Zhang, Divertor of the European DEMO: engineering and technologies for power exhaust, Fus. Eng. Des. 175 (2022) 113010, https://doi.org/10.1016/j.fusengdes.2022.113010.
[7] S. Noce, G. Dose, D. Flammini, V. Imbriani, G. Mazzone, F. Moro, S. Roccella, F. Romanelli, R. Villari, E. Visca, J.-H. You, Nuclear analyses for the design of the ITER-like plasma facing components vertical targets of the DEMO divertor, Fus. Eng. Des. 155 (2020) 111730, https://doi.org/10.1016/j.fusengdes.2020.111730.
[8] M. Nakamichi, J.H. Kim, D. Wakai, K. Yonehara, Development of a synthesis method of beryllides as advanced neutron multiplier for DEMO reactors, Fus. Eng. Des. (2012) 896–899, https://doi.org/10.1016/j.fusengdes.2012.02.053.
[9] T. Hoshino, M. Nakamichi, Development of fabrication technologies for advanced breeding functional materials For DEMO reactors, Fus. Eng. Des. 87 (2012) 486–492, https://doi.org/10.1016/j.fusengdes.2012.01.005.
[10] T. Hoshino, M. Nakamichi, Development of fabrication technologies for advanced breeding functional materials for DEMO reactors, Fus. Eng. Des. (2012) 486–492, https://doi.org/10.1016/j.fusengdes.2012.01.005.
[11] J.-H. Kim, S. Nakano, M. Miyamoto, M. Nakamichi, A recycling process on vanadium beryllium intermetallic compounds as advanced neutron multipliers for DEMO fusion applications, Fus. Eng. Des. 162 (2021) 112124, https://doi.org/10.1016/j.fusengdes.2020.112124.
[12] P. Liu, W.L. Ding, J.D. Ji, Y.T. Song, P.T. Wang, X.B. Peng, Q.H. Chen, X. Mao, X. Y. Qian, J.W. Zhang, Heat transfer and thermo-mechanical analyses of W/CuCrZr monoblock divertor in subcooled flow boiling, Fus. Eng. Des. 144 (2019) 46–56, https://doi.org/10.1016/J.FUSENGDES.2019.04.029.
[13] P. Liu, X. Qian, X. Mao, W. Song, X. Peng, Study on creep-fatigue of heat sink in W/CuCrZr divertor target based on a new approach to creep life, Nucl. Mater. Energy 25 (2020) 100846, https://doi.org/10.1016/J.NME.2020.100846.
[14] I. Izaguirre, J. de Prado, M. Sánchez, D. Salazar, A. Ureña, Development of flexible filler ribbons by melt spinning for joining W to CuCrZr material for heat sink application, Fus. Eng. Des. 181 (2022) 113214, https://doi.org/10.1016/J.FUSENGDES.2022.113214.
[15] O. Kachko, A. Puype, D. Terentyev, C.-C. Chang, M. Rieth, R.H. Petrov, Impact of neutron irradiation on the tensile properties of advanced EUROFER97 - type steels, J. Nucl. Mater. (2024) 155176, https://doi.org/10.1016/j.jnucmat.2024.155176.
[16] S. Kano, H. Yang, J. McGrady, Y. Watanabe, M. Ando, D. Hamaguchi, T. Nozawa, H. Tanigawa, K. Yoshida, T. Shibayama, H. Abe, Radiation-induced amorphization of M23C6 in F82H steel: an atomic-scale observation, J. Nucl. Mater. 558 (2022) 153345, https://doi.org/10.1016/j.jnucmat.2021.153345.
[17] J. de Prado, M. Roldán, M. Sánchez, V. Bonache, J. Rams, A. Ureña, Interfacial characterization by TEM and nanoindentation of W-Eurofer brazed joints for the first wall component of the DEMO fusion reactor, Mater. Charact. 142 (2018) 162–169, https://doi.org/10.1016/j.matchar.2018.05.035.
[18] H. Yang, Z. Shao, Q. Lu, C. Cui, L. Xu, G. Yang, Development of reduced-activation and radiation-resistant high-entropy alloys for fusion reactor, Int J Refract Metals Hard Mater 121 (2024) 106674, https://doi.org/10.1016/j.ijrmhm.2024.106674.
[19] X. Wang, Y. Shu, L. Ma, F. Guo, Study of silver-copper-palladium solder properties for vacuum electronic devices, in: Proceedings of the Electronic Packaging Technology Conference, EPTC, 2014, pp. 167–171, https://doi.org/10.1109/ICEPT.2014.6922629.
[20] Q. Luo, S. Xue, J. Wu, Influences of Sn on properties of Ag-based and Cu-based brazing filler metals, Cryst. (Basel) 11 (2021) 1403, https://doi.org/10.3390/CRYST11111403.
[21] Z. Zhong, H.C. Jung, T. Hinoki, A. Kohyama, Effect of joining temperature on the microstructure and strength of tungsten/ferritic steel joints diffusion bonded with a nickel interlayer, J. Mater. Process. Technol. 210 (2010) 1805–1810, https://doi.org/10.1016/j.jmatprotec.2010.06.012.
[22] M. Sánchez, M.A. Garrido, C.J. Múnez, J. Rams, A. Ureña, Analysis of the brazeability of W-W joints using a high temperature Ni-based alloy, Mater. Des. 54 (2014) 900–905, https://doi.org/10.1016/j.matdes.2013.08.106.
[23] V. Díaz-Mena, J. de Prado, M. Roldán, I. Izaguirre, M. Sánchez, M. Rieth, A. Ureña, Numerical and experimental development of cupronickel filler brazed joints for divertor and first wall components in DEMO fusion reactor, J. Nucl. Mater. 588 (2024) 154830, https://doi.org/10.1016/j.jnucmat.2023.154830.
[24] G.H. Han, H. Bian, H.Y. Zhao, X.G. Song, Y. Li, D. Liu, J. Cao, J.C. Feng, Interfacial microstructure and mechanical properties of TZM alloy and ZrC particle reinforced tungsten composite joint brazed using Ti-61Ni filler, J. Alloy. Compd. 747 (2018) 266–275, https://doi.org/10.1016/J.JALLCOM.2018.02.258.
[25] J. de Prado, M. Sánchez, I. Izaguirre, D. Swan, A. Ureña, Exploring Cu-Ge alloys as filler materials for high vacuum brazing application of W and CuCrZr, Mater. Today Commun. 33 (2022) 104286, https://doi.org/10.1016/j.mtcomm.2022.104286.
[26] Anon. Plansee | Strong metals for strong products | Plansee, (n.d.). https://www.plansee.com/ (accessed September 29, 2022).
[27] M. Rieth, M. Schirra, A. Falkenstein, P. Graf, S. Heger, H. Kempe, R. Lindau, H. Zimmermann, EUROFER 97 Tensile, Charpy, Creep and Structural Tests, 2003.
[28] Anon. Silver Brazing Alloys - LOT-TEK GmbH, (n.d.). https://www.lot-tek.de/en/leistungen/Silver-brazing-alloys/ (accessed October 10, 2022).
[29] Anon. Gold Brazing Alloys - LOT-TEK GmbH, (n.d.). https://www.lot-tek.de/en/brazing-alloys/gold-brazing-alloys/ (accessed October 10, 2022).
[30] Anon. Metal Foils, (n.d.). https://www.auerhammer.com/en/products-service/metal-foils.html (accessed October 10, 2022).
[31] J. de Prado, M. Sánchez, A. Ruiz, A. Ureña, Effect of brazing temperature, filler thickness and post brazing heat treatment on the microstructure and mechanical properties of W-Eurofer joints brazed with Cu interlayers, J. Nucl. Mater. 533 (2020), https://doi.org/10.1016/j.jnucmat.2020.152117.
[32] J. De Prado, M. Sánchez, A. Urea, Development of brazing process for W-EUROFER joints using Cu-based fillers. Phys Scr, Institute of Physics Publishing, 2016 014022, https://doi.org/10.1088/0031-8949/T167/1/014022.
[33] Anon. Standard Test Method for Knoop and Vickers Hardness of Materials, (n.d.). https://www.astm.org/e0384-11.html (accessed December 23, 2022).
[34] Y.K. Yu, D.W. Liaw, R.K. Shiue, Infrared brazing Inconel 601 and 422 stainless steel using the 70Au-22Ni-8Pd braze alloy, J. Mater. Sci. 40 (2005) 3445–3452, https://doi.org/10.1007/s10853-005-0446-9.
[35] I. Izaguirre, M. Roldán, J. de Prado, V. Bonache, M. Sánchez, A. Ureña, S/TEM examination and nanomechanical response of W-Eurofer joints brazed with Cu interlayers, Nucl. Mater. Energy 31 (2022) 101155, https://doi.org/10.1016/j.nme.2022.101155.
[36] R.K. Choudhary, A. Laik, P. Mishra, Microstructure evolution during stainless steel-copper vacuum brazing with a Ag/Cu/Pd filler alloy: effect of nickel plating,

J. Mater. Eng. Perform. 26 (2017) 1085–1100, https://doi.org/10.1007/s11665-017-2553-6.